In situ Analysis of Breast Cancer Progression in Murine Models Using a Macroscopic Fluorescence Imaging System

Alicia L. Carlson, MS,[1] Michaela R. Hoffmeyer, MA,[2] Kristin M. Wall,[1] Paige J. Baugher, PhD,[2] Rebecca Richards-Kortum, PhD,[1] and Suranganie F. Dharmawardhane, PhD[2,3]*

[1]*Department of Biomedical Engineering, The University of Texas at Austin, Austin, Texas 78712*
[2]*Molecular Cell and Developmental Biology Section, Institute for Cellular and Molecular Biology, The University of Texas at Austin, Austin, Texas 78712*
[3]*Department of Anatomy and Cell Biology, Universidad Central del Caribe School of Medicine, Bayamon, Puerto Rico 00960*

Background and Objective: The goal of this study was to use an inexpensive macroscopic imaging system to monitor tumor progression in mouse models in real-time with minimal intervention.

Study Design/Materials and Methods: Illumination is provided via a xenon arc lamp and a fiber optic probe which delivers white light or quasi-monochromatic excitation via specific bandpass filters. Fluorescence emission from SCID and nude mice following mammary fat pad injection of red fluorescence protein (RFP)-expressing human breast cancer cell lines was recorded and quantified using a single lens reflex (SLR) digital camera.

Results: This simple system enabled the verification of successful tumor take and temporal quantification of tumor progression in mouse models.

Conclusion: The macroscopic fluorescence imaging system represents an inexpensive and portable tool to facilitate non-invasive in situ cancer detection with the potential to monitor fluorescent tumor formation and investigation of the efficacy of potential cancer therapeutics. Lasers Surg. Med. 38:928–938, 2006. © 2006 Wiley-Liss, Inc.

Key words: fluorescence imaging; intravital imaging; breast cancer; mouse models

INTRODUCTION

Breast cancer is estimated to account for 32% of the new cancer cases in woman in 2005 and is the second major cause of cancer deaths after lung cancer. If diagnosed early, while the disease is still localized to one area with no distant metastases, the 5-year survival rate is 97.9%. However, as the disease progresses to include surrounding tissues and distant metastases, the survival rate falls to 26.1%. The metastatic spread of breast cancer complicates treatment and lowers patient prognosis drastically [1]. The use of mouse models is a common and effective research tool to study breast cancer progression, potential oncogenes and tumor suppressors involved in the metastatic process, and to investigate prospective therapeutics to specifically target metastatic spread [2–5]. Conventional methods for studying cancer progression and therapeutic agent efficacy include end point analysis of metastases following primary mammary tumor induction in mouse models.

Analyzing tumor progression and the efficacy of therapies via these conventional methods has many limitations. Specifically, mouse mammary fat pad injection does not always lead to 100% successful tumor establishment. Verification of successful tumor establishment requires observation of the injection site for visible and palpable growth over several weeks. Scar tissue formation at the site of injection can often obscure this examination. Analysis of the efficacy of therapies and identification of potential metastatic sites for further histological examination is difficult for those not trained in pathology and often must occur after mouse sacrifice. Therefore, our goal was to adapt a macroscopic imaging system to verify successful mammary fat pad tumor implantation and monitor tumor growth over time.

We describe a preliminary study using an inexpensive macroscopic imaging system for real-time in vivo image analysis of tumor formation by red fluorescent protein (RFP) expressing breast cancer cells in mice. This system used a fiber optic probe to deliver excitation light to the mouse in order to verify successful mammary fat pad tumor take and

Abbreviations Used: RFP, red fluorescent protein; GFP, green fluorescent protein; SLR, single lens reflex.

Alicia L. Carlson and Michaela R. Hoffmeyer contributed equally to the manuscript.

Contract grant sponsor: NSF/Integrative Graduate Education; Contract grant sponsor: The Department of Defense /BCRP Pre-Doctoral Fellowship; Contract grant number: #BC031906 to M.H; Contract grant sponsor: NIH/National Institute of Cancer Research; Contract grant number: R01CA103830 to R.R.K; Contract grant sponsor: The Department of Defense/BCRP; Contract grant number: #DAMD17-02-1-0582; Contract grant sponsor: American Institute of Cancer Research 03-31-06; Contract grant sponsor: Whitaker Foundation/UT Austin Biomedical Engineering Department; Contract grant sponsor: NCRR/NIH; Contract grant number: 2G12RR03035 to UCC.

*Correspondence to: Dr. Suranganie F. Dharmawardhane, Department of Anatomy and Cell Biology, Universidad Central del Caribe School of Medicine, P.O. Box 60327, Bayamon, PR 00960-6032.
E-mail: surangi@mail.utexas.edu, surangi@uccaribe.edu

Accepted 18 August 2006
Published online 16 November 2006 in Wiley InterScience (www.interscience.wiley.com).
DOI 10.1002/lsm.20409

temporally monitor tumor progression via fluorescence intensity. This method allowed us to confirm tumor take and tumor progression before visual and palpable evidence of the tumor became available. Images were acquired with a digital single lens reflex (SLR) camera with an exposure time of 8 seconds or less per image. The short image acquisition time allowed us to image the mice using only physical restraint without the need for anesthesia, which permitted more frequent imaging than would be allowed if the animals were anesthetized for each imaging session. The macroscopic fluorescence imaging system thus represents an inexpensive and portable tool to facilitate in situ cancer detection without the need to anesthetize the animal.

MATERIALS AND METHODS

Cell Culture

The SUM 149 inflammatory breast cancer (IBC) cell line used for the study was developed from pleural effusions of breast cancer patients [6,7] and was a generous gift of Dr. Stephen Ethier, The University of Michigan, MI. SUM 149 cells were cultured in F-12 Hams medium (Gibco^{TM}, Carlsbad, CA) supplemented with 5% fetal bovine serum (Tissue Culture Biologicals, Tulare, CA), insulin, and hydrocortisone, and were cultured in a humidified 5% CO_2 atmosphere at 37°C. The human breast cancer cell line MDA-MB-435α6HG6 was selected according to α6 expression and metastatic efficiency in the nude mouse model as described in Reference [8] and was the kind gift of Dr. Janet E. Price, MD Anderson Cancer Center, Houston, TX. MDA-MB-435α6HG6 cells were cultured in Dulbecco's modified Eagle's medium (DMEM) (Gibco^{TM}, CA) with 10% fetal bovine serum (Tissue Culture Biologicals, CA) and cultured in a humidified 5% CO_2 atmosphere at 37°C.

Vector Construction

SUM 149 cells were transfected with pIRESneo2 DsRed2 (*Discosoma sp.*, RFP) and the MDA-MB-435 α6HG6 cells were transfected with pIRESpuro3 DsRed2 (RFP) using Lipofectamine as per the manufacture's protocol (Invitrogen, Carlsbad, CA). RFP-SUM 149 cells were selected in neomycin and RFP-MDA-MB-435-α6HG6 cells were selected in puromycin. The MDA-MB-435α6HG6 cells stably expressing RFP were further selected via flow cytometry. RFP expression of both cell lines remained stable at approximately 99% expression in cells that were maintained for 2–3 months in cell culture and approximately 95% in cell lines that were restarted following storage in liquid nitrogen for at least a year.

Macroscopic Imaging System

A schematic of the macroscopic imaging system is shown in Figure 1. Light from a 300 W Xenon arc lamp with an integrated parabolic reflector (Perkin Elmer, Wellesley, CA) was directed by a cold mirror to the excitation filter wheel (Oriel Instruments, Stratford, CT). The cold mirror rejected radiation below 300 nm and above 625 nm, preventing ultraviolet and infrared radiation from reaching the excitation filter. A bandpass filter centered at 545 nm with a bandwidth of 30 nm was used to select the desired excitation wavelengths (HQ545/30x, Chroma Technology, Rockingham, VT). One filter slot remained open for white light illumination to visualize the position of the mouse. Excitation light was focused onto a flexible fiber optic light guide 5 mm in diameter and 2.5 m long (Multimode Fiber Optics Inc., East Hanover, NJ) for delivery to the mouse. With the 545 nm excitation filter in place, approximately 75 mW of light exited the light guide and diverged rapidly to illuminate a large region of the mouse. The intensity incident on the mouse was 10 mW/cm^2. Fluorescence emission from the mouse was recorded using a Canon EOS-D30 digital SLR camera equipped with two emission filters, a bandpass filter centered at 610 nm with a bandwidth of 75 nm (HQ610/75m, Chroma Technology) and a 570 nm longpass filter (Schott OG570, Newport Industrial Glass,

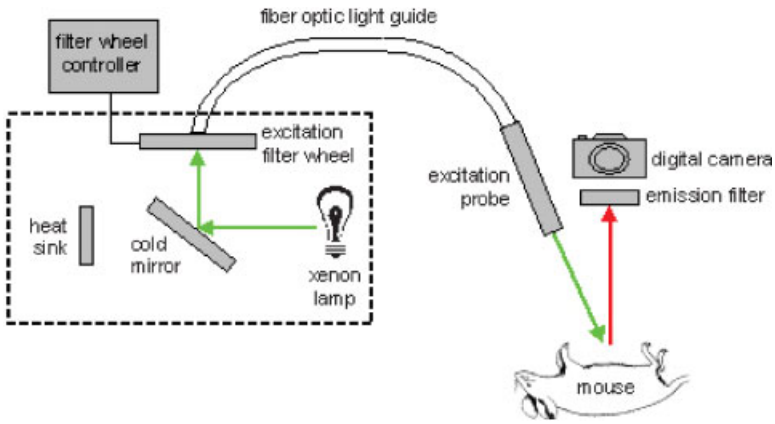

Fig. 1. Schematic of macroscopic fluorescence imaging system. Light from a Xenon arc lamp is directed by mirror to the excitation filter wheel with a bandpass filter centered at 545 nm. Excitation light enters a flexible fiber optic light guide for delivery to the mouse. Fluorescence emission from the mouse is recorded using a digital SLR camera fitted with two emission filters, a bandpass filter centered at 610 nm and a 570 nm longpass filter.

Inc., Stantor, CA), attached prior to the camera lens. The filters were easily removed for imaging with white light illumination.

The excitation and emission bandpass filters were chosen based on peak excitation and fluorescence emission wavelengths from RFP-SUM 149 cells in suspension, as demonstrated by their excitation–emission matrix (Fig. 2). The peak excitation for the DsRed RFP is 560 nm and the peak emission is 585 nm. In order to excite as much of the RFP as possible, a bandpass filter ranging from 530 to 560 nm was chosen for the excitation filter. Due to the small Stoke's shift between the excitation and emission peaks, a bandpass filter ranging from 579 to 647 nm was chosen for the emission filter, to gather the peak emission from the RFP without allowing any of the excitation light to leak through.

In vivo Imaging of RFP-Expressing Cells

All mouse experiments were approved by and performed in accordance with the Institutional Animal Care and Use Committee (IACUC) at The University of Texas at Austin. For in vivo imaging of SUM 149 breast cancer progression, 1×10^6 cells of RFP-SUM 149 or non-RFP expressing parental SUM 149 cells suspended in PBS were injected into the mammary fat pad of three 6-week-old female severe combined immunodeficient (SCID) mice (CBySmn.CB17-*Prkdc*^{scid}/J, Charles Rivers, MA) per group. Only one mouse per group was followed through the entirety of the study due to early death and problems with tumor take. For image analysis of MDA-MB-435 breast cancer progression, 2×10^6 RFP-MDA-MB-435α6HG6 cells suspended in PBS were injected into the mammary fat pad of three 6-week-old female nude immunocompromised mice (nu/nu, Charles Rivers, MA). Tumors were established in two mice which were used for the study.

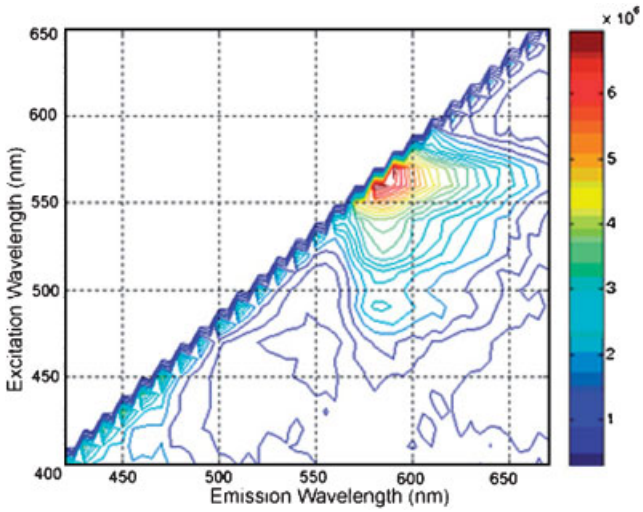

Fig. 2. Excitation–emission matrix for RFP-expressing SUM 149 cells. Fluorescence intensity is plotted as a function of excitation and emission wavelengths for the RFP-expressing SUM 149 cells in suspension. Contour lines connect points of equal fluorescence intensity and display the RFP peak excitation and emission wavelengths at 560 and 585 nm, respectively.

The areas surrounding the tumors in the SCID mice were shaved with an electric razor prior to imaging. Mice were manually restrained and imaged under white light illumination to define the animal's position. After fitting the camera with the emission filter, the mice were imaged under RFP excitation light. Images were obtained at multiple exposure times, ranging between 1 and 8 seconds, from each animal. Positive and negative standards were also imaged at the same set of exposure times under the same conditions as the mouse at each imaging session. Rhodamine, a stable laser dye, was used as the positive standard and a frosted cuvette was used as the negative standard. Imaging occurred 2–3 times per week.

Digital images were checked for saturation in each color channel. Unsaturated images of the RFP mice with the longest exposure time were chosen for further analysis. Images corresponding to the same exposure time were chosen for the control mice and the Rhodamine standard. These images were converted to grayscale using Matlab (The MathWorks, Natick, MA). The tumor area was manually traced in each grayscale image three separate times by one investigator. The fluorescence from the RFP tumors was outlined by hand based on the signal from the RFP cells. The boundary of the tumor was defined where there was at least a 1.25-fold increase in signal across the boundary. The standard deviation of the intensity of the regions on each side of the boundary did not overlap, showing confidence in the chosen boundary. Additionally, there was at least a 1.5-fold increase in the average intensity of the entire tumor region compared to the surrounding background. The tumor area of the non-RFP control animals was more difficult to outline. Since the tumor could not be defined by a region of fluorescence, the corresponding white light images were overlaid onto the fluorescence images, and the region of cell injection was traced. As the tumor grew, the tumor visualized in the white light image was outlined in the fluorescence image. The traced tumor area (in pixels) and average intensity were acquired through the Image J software (NIH, Bethesda, MD).

The average tumor fluorescence intensity was then normalized to account for the different exposure times used and any variation in light intensity by dividing the average intensity of the tumor by the average Rhodamine intensity at the same exposure time. The normalized grayscale intensity value of the tumor was then plotted versus time. The traced tumor area was converted from pixels to mm^2, using an image of a ruler to define the mm/pixel ratio, and plotted versus time.

RESULTS

To verify the expression of RFP and the lack of fluorescence in the parental, non-RFP breast cancer cells, we viewed cell pellets containing 4×10^6 cells with the macroscopic imaging system prior to mammary fat pad

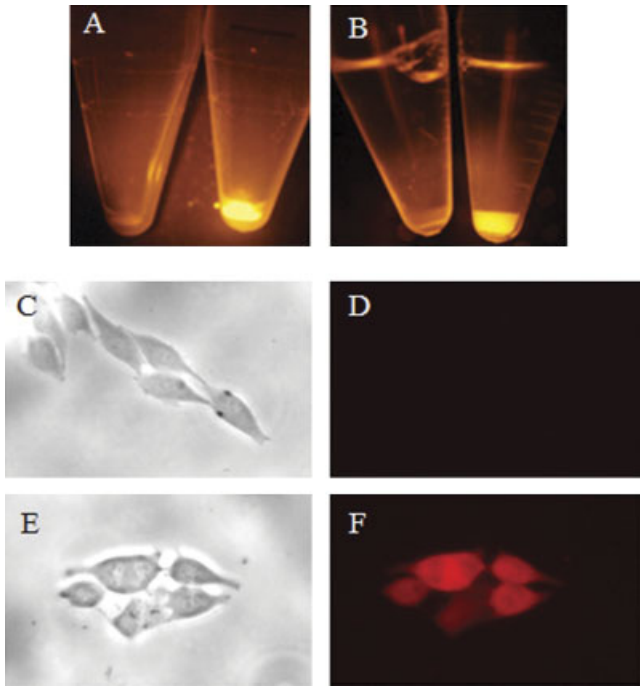

Fig. 3. Verification of red fluorescence of human breast cancer cells stably expressing RFP. **A**: Fluorescence images of cell pellets (4×10^6 cells) of non-RFP (left tube) or RFP-tagged (right tube) SUM 149 cells using the macroscopic imaging system. **B**: Fluorescence images of cell pellets (4×10^6) of non-RFP (left tube) and RFP-tagged (right tube) MDA-MB-435α6HG6 cells. **C**: Bright field micrograph of non-RFP MDA-MB-435α6HG6 cells at 100× magnification. **D**: Fluorescence micrograph of non-RFP MDA-MB-435α6HG6 cells at 100× magnification. **E**: Bright field micrograph of RFP-tagged MDA-MB-435α6HG6 cells at 100× magnification. **F**: Fluorescence micrograph of RFP-tagged MDA-MB-435α6HG6 cells at 100× magnification. [Figure can be viewed in color online via www.interscience.wiley.com.]

injection (Fig. 3A,B). All of the RFP-tagged breast cancer cells that were used for this study expressed RFP at a 99–100% efficiency. Figure 3A illustrates cell pellets viewed under RFP excitation for SUM 149 (Fig. 3A left tube) and RFP-tagged SUM 149 (Fig. 2A right tube) cells. MDA-MB-435α6HG6 cells were also pelleted (Fig. 3B left tube) and imaged along side a RFP-tagged MDA-MB-435α6HG6 cell pellet (Fig. 3B right tube). No fluorescent signal was detected under RFP excitation by our system for either of the parental, non-RFP-expressing cell lines. RFP and parental MDA-MB-435α6HG6 cells were also imaged by fluorescence microscopy (Fig. 3D and F). Again, no RFP fluorescence was detected under 100× magnification from the parental cell line (Fig. 3D) while the RFP-tagged MDA-MB-435α6HG6 cells exhibited uniform red fluorescence at 100% efficiency (Fig. 3F).

Figure 4 represents white light and fluorescent images of stably expressing RFP-SUM 149 IBC human breast cancer establishment and progression in the mammary fat pad of female SCID mice. White light images represent the location and relative size of the mammary tumor. Nodules, such as the one observed in the white light image at 2 days after mammary fat pad injection, may represent scar tissue or inflammation rather than an actual tumor. Using our macroscopic fluorescence imaging system to excite RFP fluorescence, we were able to visualize the site of breast cancer cell injection in the mammary fat pad and tumor take and survival in the SCID mouse host staring from time of injection. At Day 2, potential tumor formation at the injection site was evident in the fluorescence image. At Day 21, the fluorescence image shows successful mammary tumor establishment after a slight decrease in the fluorescence intensity due to the death of some of the injected cells. At Day 35, the same tumor demonstrated a substantial increase in red fluorescence and a discernable mammary tumor in the corresponding white light image (Fig. 4A).

In parallel, female SCID mice were also injected in the mammary fat pad with non-RFP-expressing SUM 149 human breast cancer cells. Two days post-injection, a region of potential mammary tumor formation by the injected non-fluorescent breast cancer cells was perceived in the white light image and, as expected, there was no detectable fluorescence signal under RFP excitation illumination. By Day 34, a non-RFP-expressing SUM 149 tumor was clearly visible under white light in the mammary fat pad of the SCID mouse. As expected, no RFP emission was detected under fluorescence imaging (Fig. 4B).

Using the macroscopic fluorescence imaging system, we monitored RFP-tagged SUM 149 mammary tumor growth in SCID mice over time by analyzing changes in tumor fluorescence intensity. Fluorescent images of the RFP-tagged SUM 149 tumors were converted to grayscale and the fluorescent tumor area traced three separate times. The mean grayscale pixel value within the traced tumor area was normalized for variations in exposure time and light intensity, as described in Materials and Methods section, and plotted for each image (Fig. 5A). An increase in fluorescence intensity was evident with increased mammary tumor size. A small, initial decrease in fluorescence intensity was observed near Day 8; possibly due to the death of some of the injected RFP expressing cancer cells that did not successfully take within the mammary tissue. After this initial decrease, the fluorescence intensity steadily increased as the RFP-tagged tumor grew in size.

A similar analysis was conducted on images of the non-RFP-expressing SUM 149 tumors (Fig. 5A). Autofluorescence from the non-RFP-expressing tumor and overlying skin and shaved hair was substantially low compared to the RFP-tagged tumor. Interestingly, the untagged tumor exhibited diminished background fluorescence with time. This may be due to the degradation of fluorescent connective tissue components, such as collagen cross-links, during tumor progression.

In addition to measuring the increase in fluorescence intensity, the progression in mammary tumor area was determined by analyzing the number of pixels included in the tumor region defined in the fluorescence images. The

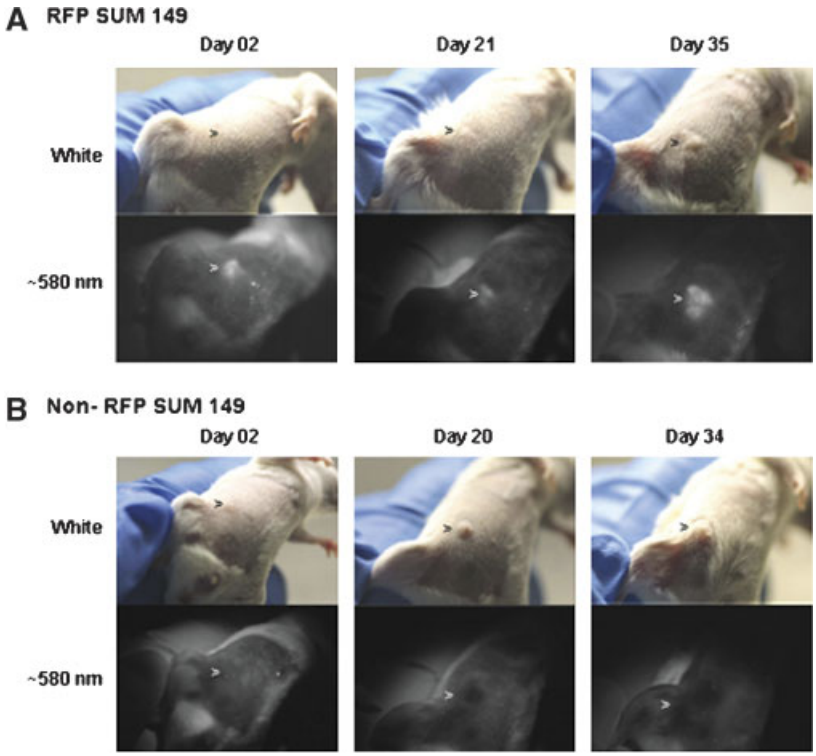

Fig. 4. Images of RFP- and non-RFP-expressing SUM 149 mammary tumors in female SCID mice. **A**: Tumors created from RFP-tagged SUM-149 cells. Top row, images under white light; bottom row, fluorescence images at 580 nm emission. Left column, 2 days; center column, 21 days; right column, 35 days following injection. Images for Day 2 were taken with 6-second exposure time and images for Days 21 and 35 were taken with 3-second exposure. **B**: Tumors created from non-RFP SUM 149 cells. Top row, images under white light; bottom row, fluorescence images at 580 nm emission. Left column, 2 days; center column, 20 days; right column, 34 days following injection. Images for Day 2 were taken with 6-second exposure time and images for Days 20 and 34 were taken with 3-second exposure. All images shown are raw images and have not been normalized. Arrowheads indicate tumor site. [Figure can be viewed in color online via www.interscience.wiley.com.]

area in pixels, as determined using Image J software, was converted to mm^2 and plotted versus time (Fig. 5B). From this analysis, the RFP-tagged SUM 149 tumor demonstrated a decrease in tumor area at Day 8, corresponding to the decrease in fluorescence intensity and the expected death of some of the injected RFP expressing cancer cells that did not successfully take within the mammary tissue. Beyond Day 8, the size of the tumor increased as a function of time until Day 44 and reached a plateau. The observed difference in the time-dependent changes of the fluorescence intensity and the tumor area are likely due to the fact that the fluorescence intensity represents fluorescence from the three-dimensional tumor whereas the traced tumor area defines the tumor as a two-dimensional object.

Tumor growth was also determined for both RFP-tagged and non-RFP-expressing tumors by a more conventional method, using caliper measurements (Fig. 5C). The fluorescence imaging system detected RFP-SUM 149 cells from Day 0. However, the tumor size could not be reliably determined by caliper measurements until Day 30 when the tumors reached a mean area of 3×3 mm^2, illustrating the utility of the imaging system for early tumor detection. The tumor site was inspected by palpation at each imaging session. When the tumors reached approximately 1–5 mm^2, they were considered large enough to measure with calipers. Caliper measurements of the RFP-SUM 149 tumor (Fig. 5C) demonstrated an increase followed by a decrease in tumor area around Day 40, similar to the corresponding area measurements derived from outlining the tumors in the fluorescence images (Fig. 5B). However, the tumor area defined by the fluorescence images was larger than the caliper measurements. Inflammatory breast cancer often manifests itself as an inflammatory response on the skin and not as a localized tumor. Therefore, tumor area measurements derived from fluorescence images may represent tumor invasion on the skin surface, which was detected by the imaging system but not by conventional caliper measurements. The tumor area defined from the images for the non-RFP-SUM 149 tumors actually yielded a slightly smaller tumor size than the caliper measurements. This is likely due to error made while outlining the tumors in the images. These data also demonstrate that the decrease in autofluorescence of the non-RFP tumor region was not due to a

decrease in tumor size because at 48 days following inoculation, the RFP-tagged tumor was 5.75×5.2 mm^2 in size while the non-RFP-expressing tumor measured at 6.4×5.8 mm^2.

Here, we have demonstrated that the macroscopic imaging system enabled a direct analysis of tumor growth over time by monitoring the increase in fluorescence signal. We also demonstrated that the RFP-expressing SUM 149 cell line successfully maintained fluorescence in a mouse over an extended period of time. As expected, the non-RFP-expressing SUM 149 mammary tumors showed no increase in fluorescence signal as the tumor increased in size over time. The low background fluorescence measured can be attributed to autofluorescence signal from fluorescent components of the skin and shaved hair of the SCID mouse. Interestingly, a modest decrease in autofluorescence intensity was seen in the non-RFP SUM 149 tumor. This may have been due to the degradation of fluorescent connective tissue components that contribute to the autofluorescence of SCID mouse skin and by an increase in angiogenesis surrounding the tumor, and thus absorption of the light by hemoglobin.

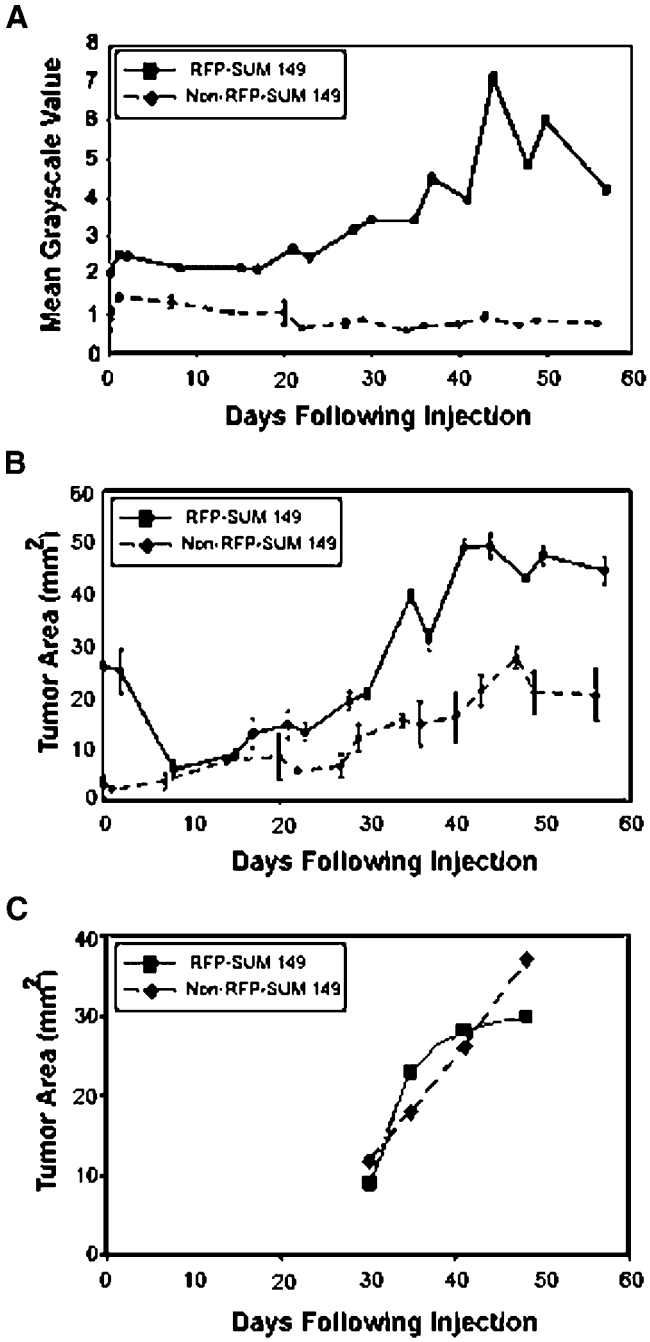

Fig. 5. Fluorescence intensity and area of RFP- and non-RFP-expressing SUM 149 mammary tumors in SCID mice as a function of time. **A**: SCID mice with RFP and non-RFP tagged SUM 149 mammary tumors were imaged under RFP excitation using the macroscopic imaging system. Images were converted to grayscale and mean grayscale pixel value from the traced tumor area was plotted versus time. Error bars indicate the standard deviation within three separate measurements of the tumor intensity. **B**: The traced tumor area was measured and converted to mm^2. The tumor area is plotted versus time. Error bars indicate the standard deviation within three separate measurements of the tumor area. **C**: The areas of same RFP and non-RFP tagged SUM 149 mammary tumors were measured using calipers starting at Day 30 following injection when the tumors were quantifiable by caliper measurements.

A similar set of experiments were performed using a highly metastatic RFP-tagged human breast cancer cell line in a different immunocompromised mouse strain to illustrate the versatility of our system. Figure 6 presents white light and fluorescent images of stably expressing RFP-MDA-MB-435α6HG6 human breast tumors in the mammary fat pad of female athymic, nude mice. In the Day 7 fluorescent image, RFP emission was obvious at the site of injection, indicating successful MDA-MB-435α6HG6 tumor cell take and survival in the nude mouse host. At Day 71, the white light image of the same mouse showed a clearly discernable mammary tumor. The image of this tumor under RFP excitation on Day 71 showed a substantial increase in fluorescence signal. In parallel, female nude mice were also injected in the mammary fat pad with non-RFP-expressing MDA-MB-435α6HG6 human breast cancer cells which emitted no fluorescence above background autofluorescence of the skin.

We monitored RFP-tagged MDA-MB-435α6HG6 mammary tumor growth in nude mice over time by analyzing increases in tumor fluorescence intensity (Fig. 7A). Parallel linear increases in fluorescence intensity as a function of time were observed for both of the RFP-expressing MB-435 tumors. Figure 7B shows the tumor area measured in the fluorescence images. The RFP-expressing tumor 1 shows an increase in tumor area with time. Tumor 2, however, does not show this same increase in area, despite the increase in fluorescence. This is due to the fact that this tumor protruded from the skin more than it spread laterally, and this three-dimensional growth was not taken

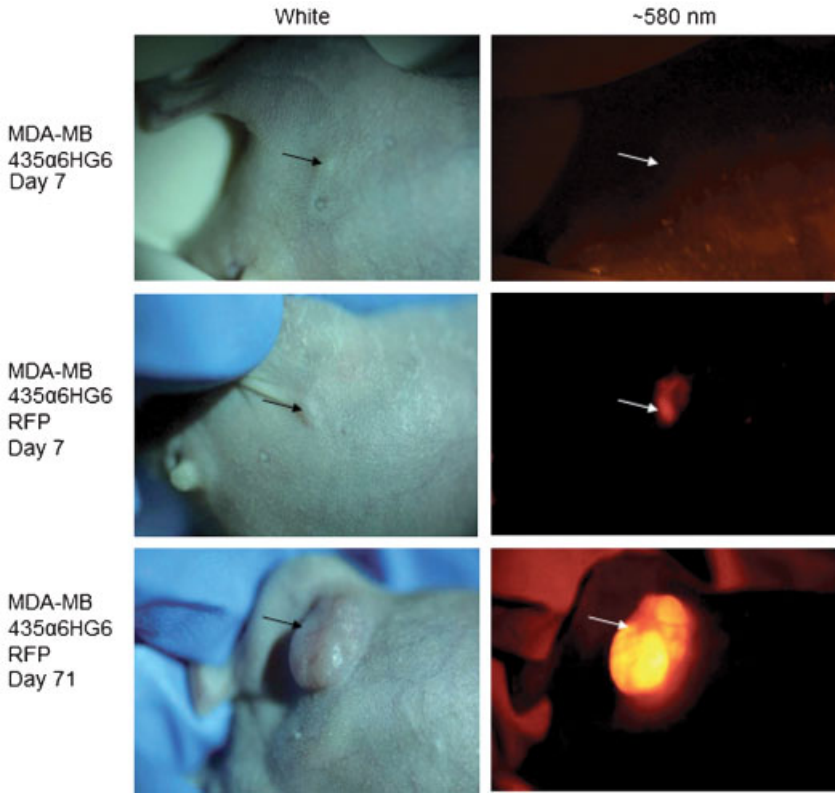

Fig. 6. Images of RFP- and non-RFP-expressing MDA-MB-435α6HG6 mammary tumors in female athymic, nude mice. Left column, images under white light; right column, fluorescence images at 580 nm emission. Top row, non-RFP-tagged MDA-MB-435α6HG6 mammary tumors. Middle row, RFP-tagged MDA-MB-435α6HG6 mammary tumor at Day 7 post-mammary cancer cell injection. Bottom row, RFP-tagged MDA-MB-435α6HG6 mammary tumor at Day 71. Images for Day 7 were taken with 8-second exposure time and images for Day 71 were taken with 1-second exposure. All images shown are raw images and have not been normalized. Arrows indicate tumor site.

into account in the two-dimensional tumor area analysis. In this case, quantification of the increase in fluorescence intensity of the tumor provided a more accurate evaluation of tumor size. Therefore, the macroscopic fluorescence imaging system can be conveniently used to non-invasively quantify fluorescent tumor progression of a metastatic breast cancer cell line.

Figure 8 presents images of distant fluorescent metastases. We were able to detect areas of distant metastases by whole-body imaging; however, intravital imaging where a skin flap is opened over the areas of interest, as described in Reference [9], was necessary for a complete analysis of metastatic lesions by the system in the current configuration. Following necropsy, red fluorescence signal from distant lung metastases was easily detected by our system; verifying the existence of metastatic lesions. Therefore this system can be easily used to detect and quantify metastases without prior histopathology.

DISCUSSION

We have detailed the utilization of a macroscopic fluorescence imaging system to monitor RFP-tagged human tumor progression in immunocompromised mice in real-time with no or minimal intervention. Using this system, we can determine if RFP-expressing human breast cancer cells have successfully established a mammary tumor in the mouse at a much earlier time than visualizing tumor growth post-injection as a means to verify successful implantation. Furthermore, such methodology can be used to monitor tumor growth over time by measuring an increase in fluorescence intensity from the RFP-tagged tumor. Finally, this system can successfully locate the fluorescence signal from metastatic tumors and thus facilitate identification of regions of interest for further examination by histopathology.

The development and optimization of this system was not without complication. The mouse diet (Harlan Teklad, Madison, WI) was found to fluoresce under excitation for RFP and can be seen in the intestinal tract of many of the mouse images (data not shown). While this did not hinder analysis of tumor take and tumor growth over time, this can easily be reduced by feeding mice a corn-based diet devoid of the chlorophyll responsible for this background fluorescence. Also, we found it necessary to use the SCID mouse for RFP-SUM 149 experiments because of limited success with tumor establishment in nude mice. To avoid the strong

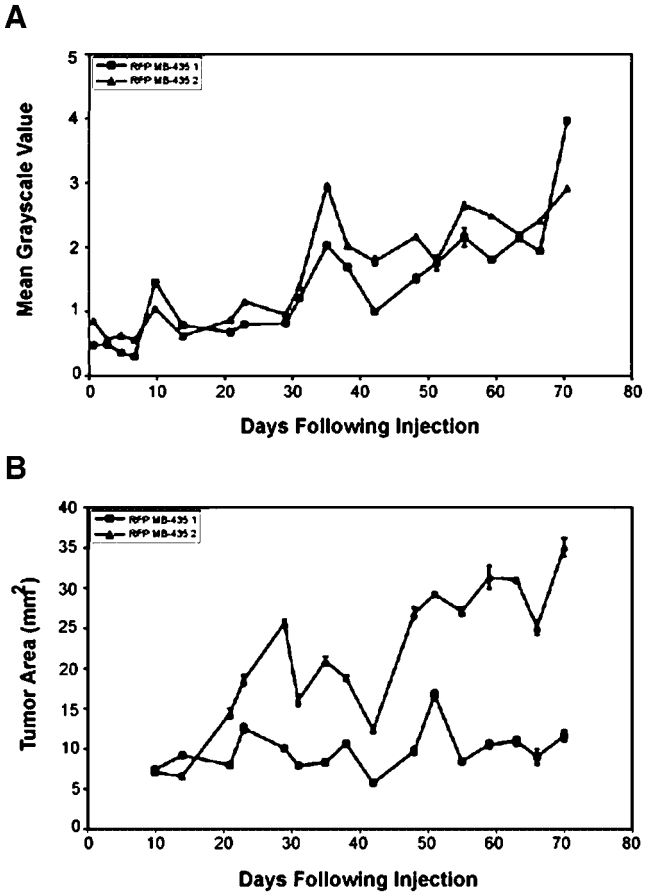

Fig. 7. Fluorescence intensity and area of RFP-expressing MDA-MB-435α6HG6 mammary tumors in nude mice as a function of time. RFP-MDA-MB-435α6HG6 cells were injected into the mammary fat pads of female athymic, nude mice. Tumor growth was monitored via fluorescent image analysis using the macroscopic imaging system. **A**: Images were converted to grayscale and the mean grayscale pixel value for the traced tumor area was plotted versus time. Figure shows two plots, both from RFP-expressing tumors. Error bars indicate the standard deviation within three separate measurements of the tumor intensity. **B**: The traced tumor area was measured and converted to mm^2. The tumor area is plotted versus time. Error bars indicate the standard deviation within three separate measurements of the tumor area.

fluorescence signal of the hair of the SCID mice, we shaved them prior to imaging. However, we could still successfully detect tumor take and monitor tumor growth over time. With the highly metastatic human breast cancer cell line RFP-MDA-MB-435α6HG6, we could utilize nude mice and successfully monitor tumor take and progression with results similar to those obtained with the RFP-SUM 149 tumors in SCID mice. Therefore, we believe this system can be successfully employed with many different mouse strains.

So far, few studies have utilized RFP to image cancer and most of these studies have used surgical orthotopic implantation (SOI) to transplant fragments of RFP-tagged tumors into rodent models [10]. Sorg et al. [11] used window chamber tumors to study RFP-tagged tumor progression by injecting a suspension of tumor cells into the dorsal skin flap prior to implanting a coverslip window over the exposed skin. In this study, we describe the use of RFP-tagged cells to establish mammary tumors in mouse models through subcutaneous injection. We used DsRed as the fluorescent tag because it fluoresces at a longer wavelength than other available fluorescent proteins, which yields reduced interference from autofluorescence of endogenous fluorophores compared to the emission wavelengths of other fluorescent proteins. DsRed (RFP) also has broader excitation and emission spectra than other fluorescent proteins, which provides a broader range of illumination and detection wavelengths that can be used with a white-light lamp excitation source. Patterson et al. reports that the extinction coefficient of green fluorescent protein (GFP) EGFP is 55,000 M^{-1} cm^{-1} and the quantum yield is 60%. Similarly, the extinction coefficient of DsRed (RFP) is 72,500 M^{-1} cm^{-1} and the quantum yield is 68% [12]. Therefore, the fluorescence intensity, the product of the extinction coefficient and the quantum yield, of DsRed is comparable to that of GFP, supporting our choice for using DsRed. One of the disadvantages of imaging DsRed is that its fluorescence emission lies within an absorption peak of hemoglobin. Therefore, some of the fluorescence is likely to be absorbed by hemoglobin in surrounding blood vessels. However, Yamauchi et al. [13] have recently shown that cells expressing RFP can be clearly imaged in a blood vessel. The sensitivity of our system to detect a minimum of 1×10^5 RFP-tagged cells in situ was moderate at 6–7 times over the autofluorescence signal, but this may be improved by the use of GFP tags as previously described [9,10,14–27], due to increased sensitivity of most detectors to green wavelengths compared to red, or improved RFP constructs.

An interesting and unexpected result of this study was a decrease in background fluorescence over time from the non-RFP mouse tumor. Although collagen fluorescence is not at its peak within the emission bandpass (589–647 nm) used, some collagen fluorescence may still be detected. Therefore, the observed decrease in fluorescence could be a result of the degradation of fluorescent collagen cross-links and extracellular matrix components as well as an increase in angiogenesis leading to an increase in the absorption of light by hemoglobin.

Imaging of optically tagged cancer cells in mice has been successfully utilized to study the growth and metastatic spread of a variety of cancers and to test the efficacy of potential chemotherapies [9,10,14–32]. Hoffman et al. employ a light box system with fiber optic probe delivery of blue light for low resolution, whole body imaging of SOI GFP- and RFP-tagged tumors in mice. This system is similar to the one used for this study but employs a cooled color charge-coupled device (CCD) for detection [9,10,14–24]. In vivo bioluminescence imaging systems, such as the one developed by Contag et al., detects light emitted from

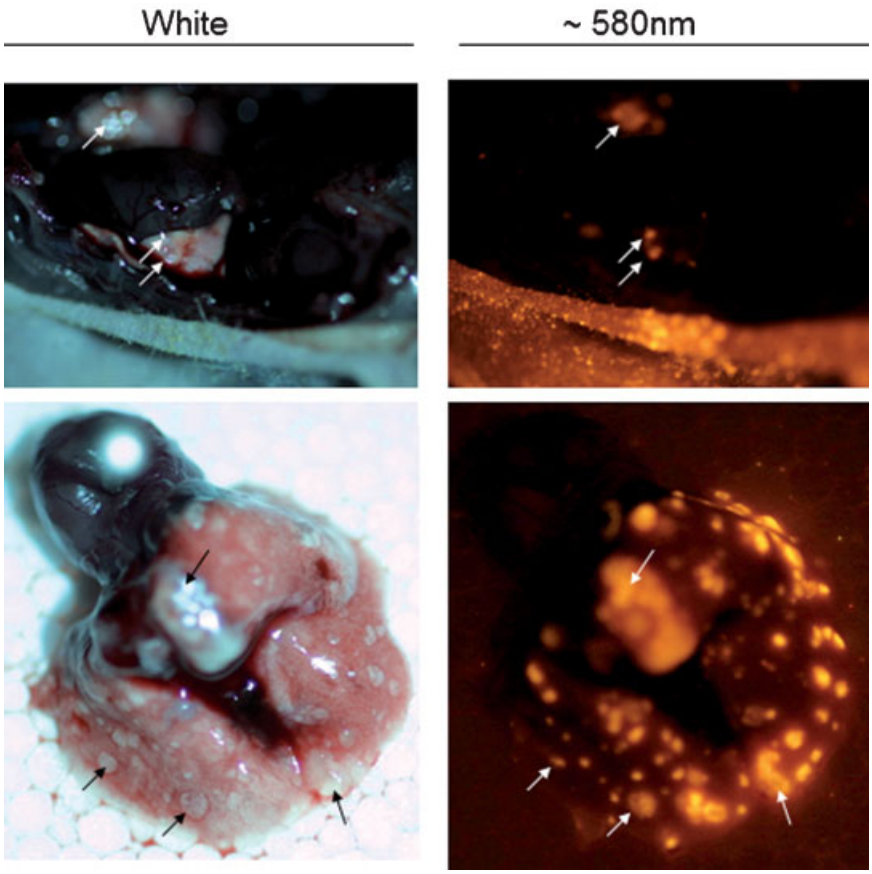

Fig. 8. Images of lung metastases from RFP-tagged MDA-MB-435α6HG6 mammary tumors. RFP-tagged MDA-MB-435α6HG6 human breast cancer cells were injected into the mammary fat pad of female, nude athymic mice. The mammary tumor was allowed to grow for 71 Days. Left column, images under white light; right column, fluorescence images at 580 nm emission. Top row, mouse with open chest cavity. Bottom row, excised lung with metastases seen as white nodules (black arrows) under white light and RFP-expressing metastatic lesions verified by fluorescent imaging (white arrows).

bioluminescent cells within mice using an intensified and/or ultra-cooled CCD camera. Bioluminescent imaging has been utilized to detect cancer cells from the time of inoculation through tumor progression and to evaluate cancer therapies [28–32]. Bioluminescent systems typically use the firefly luciferase gene as the cell reporter. In order to bioluminesce, the cells need access to oxygen to be metabolically active and require external luciferin as a substrate unless engineered to produce it in situ [29]. Luciferase produces low photon flux yielding low light levels, but signal is only produced where luciferase is present with little or no background signals, which makes this method attractive. The low photon flux produced, however, requires a light tight enclosure and a very sensitive camera capable of long exposure times, typically on the order of 1–5 minutes [28,29,33], and low thermal and read-out noises for imaging. This can be accomplished with an intensified and/or ultra-cooled CCD, but these are generally expensive cameras. Also, the long exposure times require sedation of the animal prior to imaging [9,22,23,26–28]. Fluorescence imaging of protein-tagged cells, meanwhile, requires an external light source which may induce a brighter background which arises from intrinsic autofluorescence. However, a much brighter signal is produced by the fluorescent protein-tagged cells which allow much shorter exposure times, on the order of a few seconds [34], and less sensitive cameras to be used for imaging without the need to anesthetize or sedate the animals.

The inexpensive system described herein enabled non-invasive examination of fluorescent breast cancer progression in vivo without the need for sedation of the animals. The largest advantage of our system is the fact that it uses a commercially available digital SLR camera to acquire the images rather than a CCD, which greatly reduced the overall cost of the system. Although the digital SLR camera has a lower sensitivity than the CCD, we were still able to acquire images using exposure times of 8 seconds or less per image. This in turn enabled us to image the mice using only physical restraint without the need for anesthesia. The lack

of anesthesia allowed us to image the mice every 2–3 days rather than once per week as had been done in previous studies [28,33]; yielding more data points throughout the time course of the study. More time points provide the user with more information regarding the rate of growth of the tumor and spread of the disease, and can be used to analyze the rate of reduction in the tumor size after therapy has been administered. Our system did not clearly detect distant metastases through the skin of nude mice. Use of a CCD camera would improve the sensitivity of this imaging system and extend its capabilities to noninvasively image distant metastases. However, as demonstrated in the present configuration, it can be used to conveniently image and quantify number and size of distant metastases following necropsy.

Finally, the macroscopic fluorescence imaging system described is inexpensive and easy to assemble. We utilized a consumer-grade digital SLR camera to obtain images which can be purchased for less than $800. Although we used a filtered arc lamp as a source of excitation, several inexpensive alternatives could be used. For example, excitation light can be provided by a Helium–Neon laser, a diode pumped solid state (DPSS) laser, or a Light Emitting Diode (LED). HeNe and DPSS lasers provide very narrow linewidth excitation. For lower powers, a HeNe laser costs as little as $500 (Melles Griot) and a DPSS laser can be purchased for as little at $800 (Midwest Laser). Recently, a blue LED flashlight was used as an inexpensive alternative for whole-body imaging of GFP- or RFP-tagged tumors in nude mice [24]. An LED, yielding 60 mW of power, with driver and necessary accessories costs approximately $80 (TheLEDLight.com). The total cost of our system was under $4,000, including the camera. However, if a LED is used as the excitation source rather than the arc lamp, the cost of the system decreases to under $1,850, making this a very inexpensive intravital imaging modality.

Clearly, the mouse model of breast cancer in conjunction with advances in intravital imaging affords many advantages over traditional in vitro and in vivo assays in the study of metastatic breast cancer progression. Intravital imaging can be performed with simple tools, and affords the ability to follow tumor progression over time in a single animal. Thus, studies can be carried out with fewer animals reducing artifacts due to biological variability. This macroscopic imaging system will be used in future applications to investigate the efficacy of potential anti-cancer therapies.

ACKNOWLEDGMENTS

We thank Vivian Mack for expert technical assistance and Dr. Janet Price (MD Anderson cancer Center, Houston, TX) and Dr. Stephen Ethier (University of Michigan, MI) for providing the breast cancer cell lines. NSF/Integrative Graduate Education and Research Training Fellowships to A.C. and M.H. The Department of Defense /BCRP Pre-Doctoral Fellowship #BC031906 to M.H. NIH/National Institute of Cancer Research R01CA103830 to R.R.K The Department of Defense/BCRP #DAMD17-02-1-0582. American Institute of Cancer Research 03-31-06, and Whitaker Foundation/UT Austin Biomedical Engineering Department Seed Grant to S.D., and NCRR/NIH 2G12RR03035 to UCC.

REFERENCES

1. Jemal A, Murray T, Ward E, Samuels A, Tiwari RC, Ghafoor A, Feuer EJ, Thun MJ. Cancer Statistics, 2005. CA Cancer J Clin 2005;55:10–30.
2. Killion JJ, Radinsky R, Fidler IJ. Orthotopic models are necessary to predict therapy of transplantable tumors in mice. Cancer Metastasis Rev 1999;17:279–284.
3. Price JE. Analyzing the metastatic phenotype. J Cell Biochem 1994;56:16–22.
4. Price JE. Metastasis from human breast cancer cell lines. Breast Cancer Res Treat 1996;39:93–102.
5. Price JE, Zhang RD. Studies of human breast cancer metastasis using nude mice. Cancer Metastasis Rev 1990;8:285–297.
6. Ethier SP, Kokeny KE, Ridings JW, Dilts CA. erbB family receptor expression and growth regulation in a newly isolated human breast cancer cell line. Cancer Res 1996;56:899–907.
7. Ethier SP. Human breast cancer cell lines as models of growth regulation and disease progression. J Mammary Gland Biol Neoplasia 1996;1:111–121.
8. Mukhopadhyay R, Theriault RL, Price JE. Increased levels of alpha6 integrins are associated with the metastatic phenotype of human breast cancer cells. Cell Exp Metastasis 1999;17:325–332.
9. Yang M, Baranov E, Wang JW, Jiang P, Wang X, Sun FX, Bouvet M, Moossa AR, Penman S, Hoffman RM. Direct external imaging of nascent cancer, tumor progression, angiogenesis, and metastasis on internal organs in the fluorescent orthotopic model. Proc Natl Acad Sci USA 2002;99:3824–3829.
10. Hoffman RM. Orthotopic metastatic (MetaMouse) models for discovery and development of novel chemotherapy. Methods Mol Med 2005;111:297–322.
11. Sorg BS, Moeller BJ, Donocan O, Cao Y, Dewhirst MW. Hyperspectral imaging of hemoglobin saturation in tumor microvasculature and tumor hypoxia development. J Biomed Opt 2005;10(4):044004.
12. Patterson G, Day R, Piston D. Fluorescent protein spectra. J. Cell Sci 2001;114:837–838.
13. Yamauchi K, Yang M, Jiang P, Xu M, Yamamoto N, Tsuchiya H, Tomita K, Moossa AR, Bouvet M, Hoffman RM. Development of real-time subcellular dynamic multicolor imaging of cancer-cell trafficking in live mice with a variable-magnification whole-mouse imaging system. Cancer Res 2006;66: 4208–4214.
14. Chishima T, Miyagi Y, Wang X, Yamaoka H, Shimada H, Moosa AR, Hoffman RM. Cancer invasion and micrometastasis visualized in live tissue by green fluorescent protein expression. Cancer Res 1997;57:2042–2047.
15. Yang M, Baranov E, Jiang P, Sun FX, Li XM, Li L, Hasegawa S, Bouvet M, Al-Tuwaijri M, Chishima T, Shimada H, Moossa AR, Penman S, Hoffman RM. Whole-body optical imaging of green fluorescent protein-expressing tumors and metastases. Proc Natl Acad Sci USA 2000;97:1206–1211.
16. Yang M, Baranov E, Moossa AR, Penman S, Hoffman RM. Visualizing gene expression by whole-body fluorescence imaging. Proc Natl Acad Sci USA 2000;97:12278–12282.
17. Rashidi B, Yang M, Jiang P, Baranov E, An Z, Wang X, Moossa AR, Hoffmam RM. A highly metastatic Lewis lung carcinoma orthotopic green fluorescent protein model. Clin Exp Metastasis 2000;18:57–60.
18. Hoffman RM. Orthotopic metastatic mouse models for anticancer drug discovery and evaluation: A bridge to the clinic. Invest New Drugs 2000;17:343–359.
19. Zhao M, Yang M, Baranova E, Wang X, Penman S, Moossa AR, Hoffman RM. Spatial-temporal imaging of bacterial

infection and antibiotic response in intact animals. Proc Natl Acad Sci USA 2001;98:9814–9818.
20. Yang M, Baranov E, Li XM, Wang JW, Jiang P, Li L, Moossa AR, Penman S, Hoffman RM. Whole-body and intravital optical imaging of angiogenesis in orthopically implanted tumors. Proc Natl Acad Sci USA 2001;98:2616–2621.
21. Schmitt CA, Fridman JS, Yang M, Baranov E, Hoffman RM, Lowe SW. Dissecting p53 tumor suppressor function in vivo. Cancer Cell 2002;1:289–298.
22. Yamamoto N, Yang M, Jiang P, Tsuchiya H, Tomita K, Moossa AR, Hoffman RM. Real-time GFP imaging of spontaneous HT-1080 fibrosarcoma lung metastases. Clin Exp Metastasis 2003;20:181–185.
23. Amoh Y, Li L, Yang M, Jiang P, Moossa AR, Katsuoka K, Hoffman RM. Hair follicle-derived blood vessels vascularize tumors in skin and are inhibited by Doxorubicin. Cancer Res 2005;65:2337–2343.
24. Yang M, Luiken G, Baranov E, Hoffman RM. Facile whole-body imaging of internal fluorescent tumors in mice with an LED flashlight. Biotechniques 2005;39:170–172.
25. Wyckoff JB, Jones JG, Condeelis JS, Segall JE. A critical step in metastasis: In vivo analysis of intravasation at the primary tumor. Cancer Res 2000;60:2504–2511.
26. Wang W, Wyckoff JB, Frohlich VC, Oleynikov Y, Huttelmaier S, Zavadil J, Cermak L, Bottinger EP, Singer RH, White JG, Segall JE, Condeelis JS. Single cell behavior in metastatic primary mammary tumors correlated with gene expression patterns revealed by molecular profiling. Cancer Res 2002;62:6278–6288.
27. Ahmed F, Wyckoff J, Lin EY, Wang W, Wang Y, Hennighausen L, Miyazaki JI, Jones J, Pollard JW, Condeelis JS, Segall JE. GFP expression in the mammary gland for imaging of mammary tumor cells in transgenic mice. Cancer Res 2002;62:7166–7169.
28. Edinger M, Sweeney TJ, Tucker AA, Olomu AB, Negrin RS, Contag CH. Noninvasive assessment of tumor cell proliferation in animal models. Neoplasia 1999;4:303–310.
29. Rehemtulla A, Stegman LD, Cardozo SJ, Gupta S, Hall DE, Contag CH, Ross BD. Rapid and quantitative assessment of cancer treatment response using in vivo bioluminescence imaging. Neoplasia 2000;2:491–495.
30. Edinger M, Cao YA, Verneris MR, Bachmann MH, Contag CH, Negrin RS. Revealing lymphoma growth and the efficacy of immune cell therapies using in vivo bioluminescence imaging. Blood 2003;101:640–648.
31. Mandl SJ, Mari C, Edinger M, Negrin RS, Tait JF, Contag CH, Blankenberg FG. Multi-modality imaging identifies key times for Annexin V imaging as an early predictor of therapeutic outcome. Mol Imaging 2004;3:1–8.
32. Doyle TC, Burns SM, Contag CH. In vivo bioluminescence imaging for integrated studies of infection. Cell Microbiol 2004;6:303–317.
33. Sweeney TJ, Mailander V, Tucker AA, Olomu AB, Zhang W, Cao Y, Negrin RS, Contag CH. Visualizing the kinetics of tumor-cell clearance in living animals. PNAS 1999;96:12044–12049.
34. Mahmood U, Tung C-H, Tang Y, Weissleder R. Feasibility of in vivo multichannel optical imaging of gene expression: Experimental study in mice. Radiology 2002;224:446–451.